Electronic Supplementary Material (ESI) for Analyst.

A ratiometric, fluorometric approach for surface charge mapping of biosilica features

*Mithun Parambath[±], Aneeqa Fayyaz[±], Igor Efimov, Quentin S. Hanley, Carole C. Perry**

Interdisciplinary Biomedical Research Centre, School of Science and Technology, Nottingham Trent University, Nottingham, NG11 8NS, UK

± these authors contributed equally.

**Corresponding author carole.perry@ntu.ac.uk*

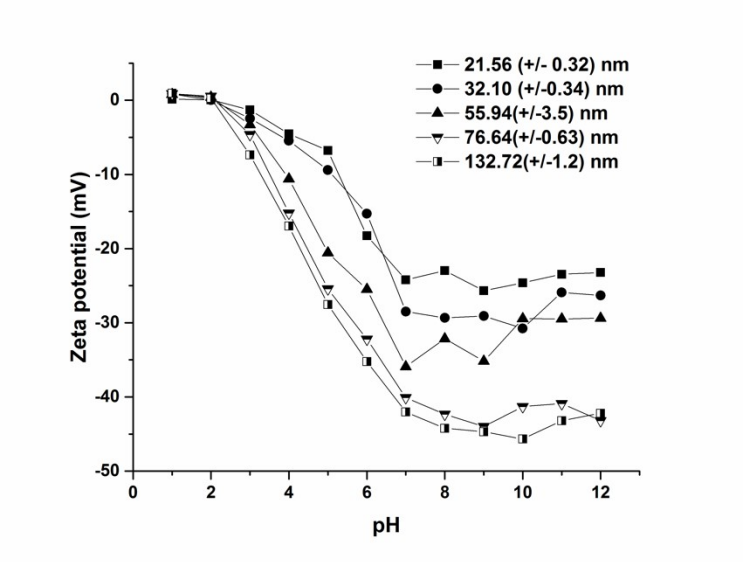

Figure S1: Zeta potential values of silica nanoparticles and their variation with pH- data collected using a microplate reader.

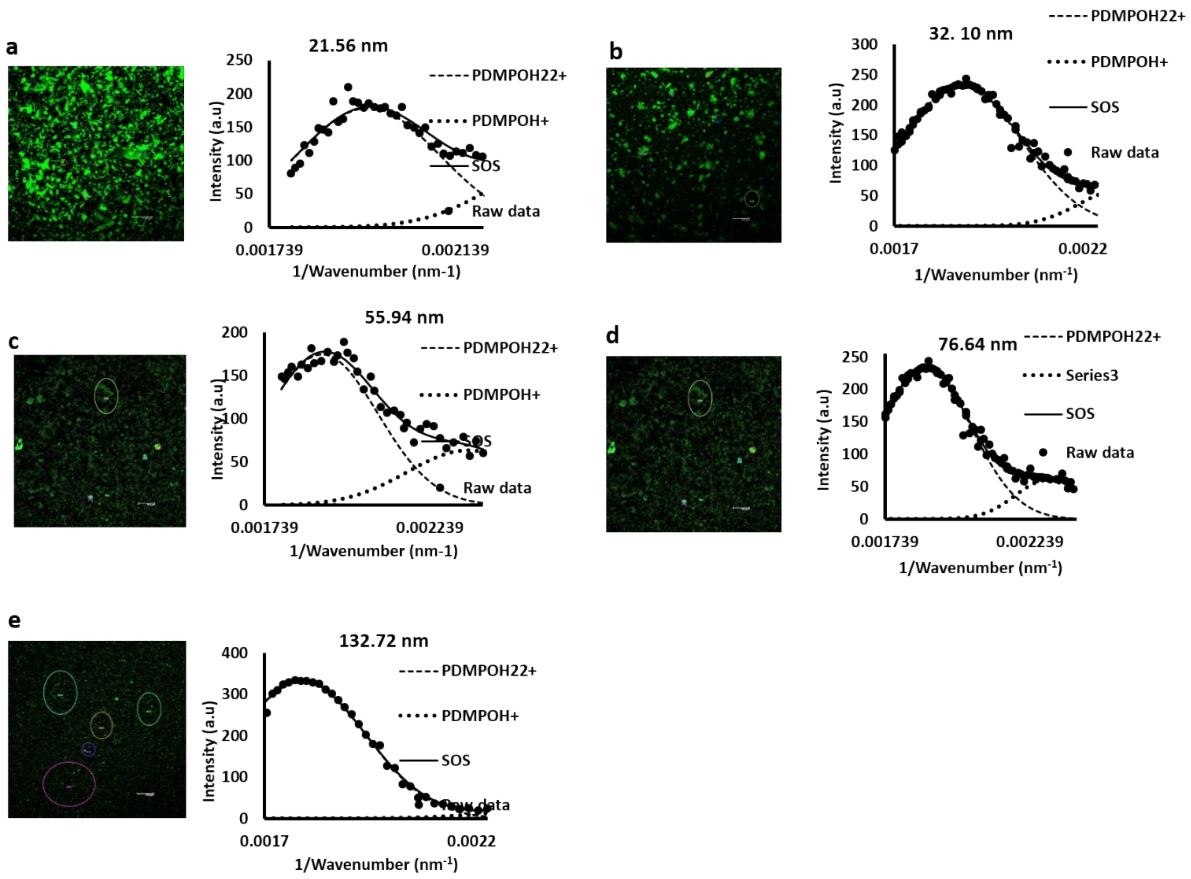

Figure S2: Confocal spectral scanning on silica nanoparticles (fixed pH) exciting at 405 nm. Confocal imaging of silica nanoparticles at pH 7.08, excited at 405 nm (left panel) and fluorescence spectrum with decomposition into two Gaussian components (right panel) (a) 21.56(+/-0.32) nm particles, (b) 32.10(+/-0.34) nm particles, (c) 55.94(+/-3.5) nm particles, (d) 76.64(+/-0.63) nm particles and (e) 132.72 (+/-1.2) nm particles.

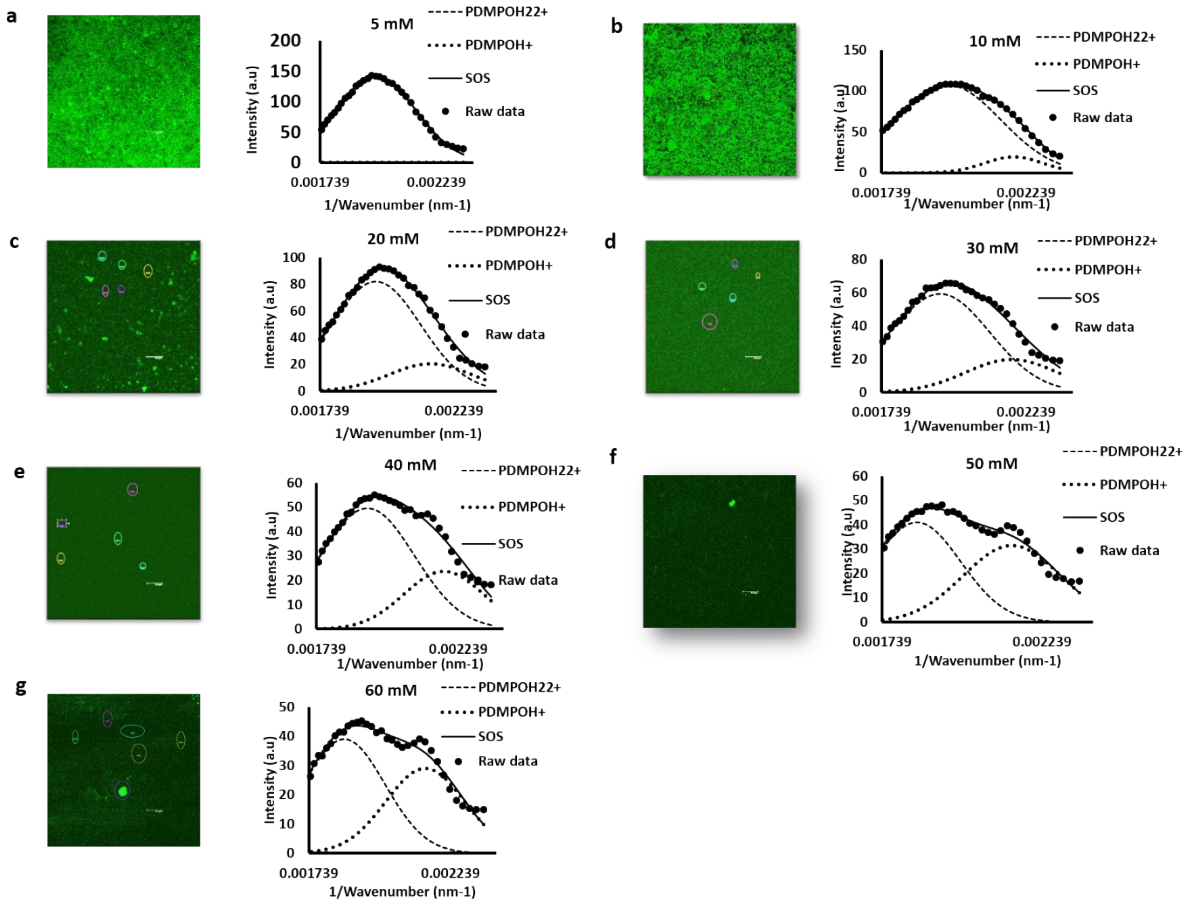

Figure S3: Fluorescence emission on Silica nanoparticles (133 nm) upon charge neutralization using GHCl at pH 7.0. Confocal imaging of silica nanoparticles excited at 405 nm and fluorescence spectrum with decomposition into two Gaussian components. Confocal imaging of silica nanoparticles excited at 405 nm (left panel) (a) SNP without GHCl (b) SNP with 10 mM GHCl (c) SNP with 20 mM GHCl (d) SNP with 30 mM GHCl (e) SNP with 40 mM GHCl (f) SNP with 50 mM GHCl (g) SNP with 60 mM GHCl.

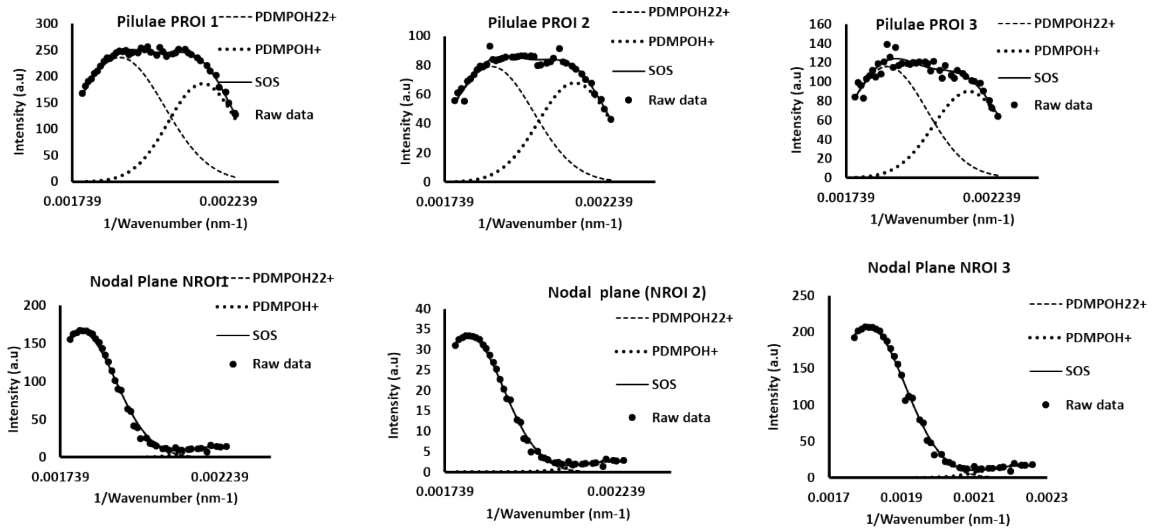

Figure S4: Charge estimation on the star-shaped rosettes and nodal plane of *Equisetum arvense* using PDMPO. Example fluorescence emission spectra collected from the star shaped rosettes (pilulae) and nodal planes Three regions of interest (ROI) are shown for each nanostructure. The fluorescence emission spectra were further subjected to Gaussian decomposition. The calculated spectra and 'goodness of 'fit' (SOS) is presented.

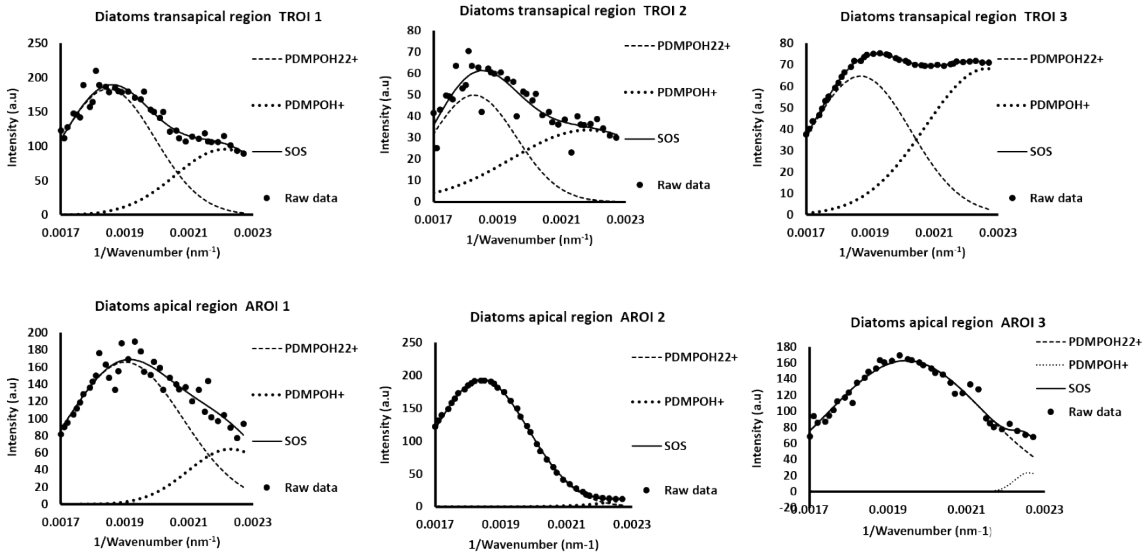

Figure S5: Charge estimation on apical and transapical axes of Nitzschia *stellata*. Example fluorescence emission spectra collected from the apical and trans apical axes of *Nitzschia stellata*. Three regions of interest (ROI) are shown for each. The fluorescence emission spectra were further subjected to Gaussian decomposition. The calculated spectra and sum of the two components (SOS) is presented.

Effects of chlorophyll on the charge mapping of *Equisetum arvense*

A stem of a growing *Equisetum arvense* plant was chopped into small pieces and treated with 10 mls of ethanol for 4 hours at room temperature to disrupt cell membranes and allow extraction of chlorophyll.[i] [ii] The fluorescence of the chlorophyll containing extract at room temperature was measured by CSLM. The emission behaviour from 440 – 850 nm nm was monitored to see if there was any overlap between the fluorescence behaviour of chlorophyll and PDMPO.[iii]

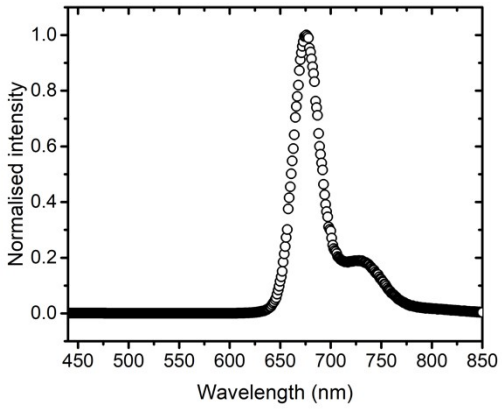

Figure S6: Normalised fluorescence emission spectrum for chlorophyll extracted from *Equisetum arvense*.

Two peaks at around 670 nm and 730 nm were observed (**Fig. S6**) which corresponded to chlorophyll. [iv] Since the contributions from chlorophyll start from after the wavelength of 630 nm, this confirmed that it would have no interference with the charge mapping measurements as the fluorescence emission spectrum data was collected within the wavelength scan ranges of 460-470 nm and 500-510 nm.

Time dependent PDMPO uptake into *Equisetum arvense*

Studying the time dependent behaviour of PDMPO uptake into *Equisetum arvense* was a crucial step towards smoothly transferring the application of the surface charge mapping to living samples. **Figure S7** shows the functional images illustrating the time dependent behaviour of PDMPO uptake into the stomata, star shaped rosette like structures (clustered pilulae) and a random array of pilulae covering the nodal plane of the cell wall of *Equisetum arvense*. (1) shows the sample without PDMPO (in water) where the observed fluorescence emission spectrum is of the background present due to the CSLM (see **Figure S7** graph 5). (2) shows the sample after two hours of PDMPO exposure where the silicified cell wall and other silicified structures start to fluoresce. This is due to the PDMPO accumulation in cellular compartments where the ratio of $(PDMPOH_2)^{2+}$) to $(PDMPOH^+)$ is highly dependent on the surrounding pH and the particle size of silica. (3) and (4) show the sample after 4 and 22 hours of PDMPO exposure respectively. A visual increase in the fluorescence emission intensity is observed over time. **Figure S7** graph 5 displays the behaviour of PDMPO uptake through the fluorescence emission spectrum where an increase in the fluorescence intensity is clearly seen. This confirms that the whole living tissue of *Equisetum arvense* is capable of up taking PDMPO depending on the silica structures present.

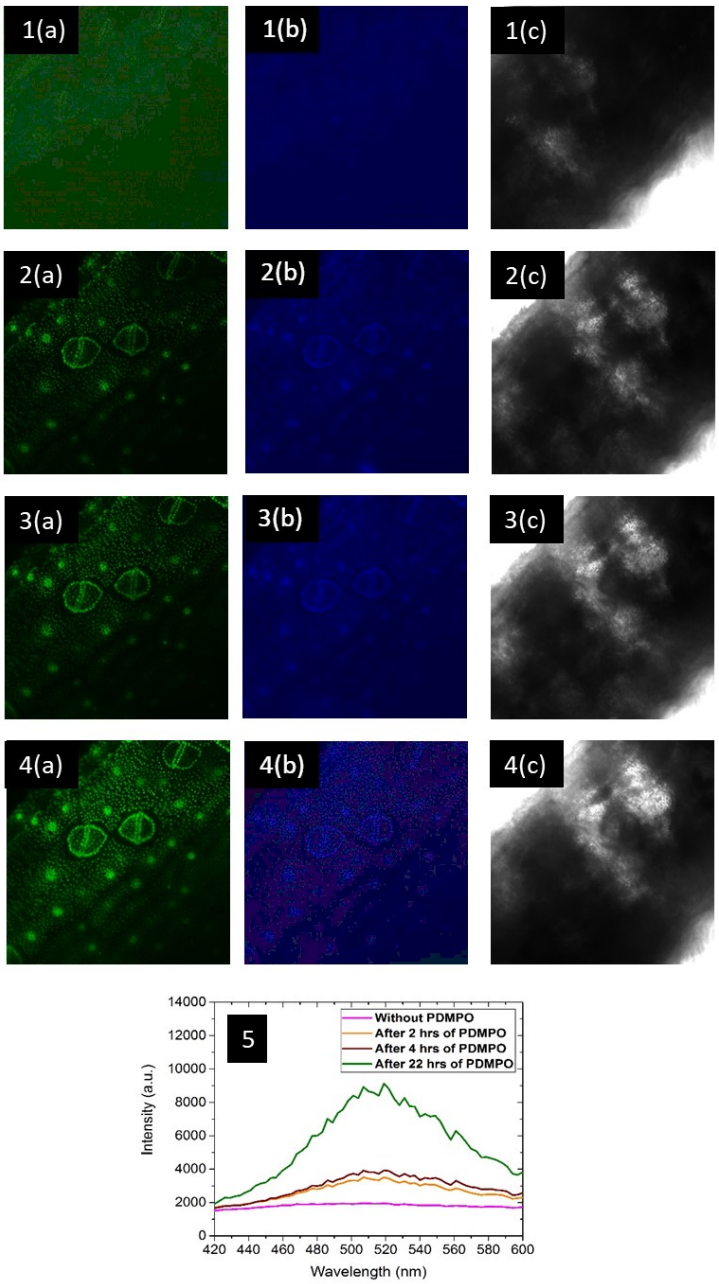

Figure S7: Functional images illustrating the time dependent behaviour of PDMPO uptake into the stomata and star shaped rosette-like structures within *Equisetum arvense.* (a) $(PDMPOH_2)^{2+}$ imaging with data collected over the wavelength range 500-510 nm, (b) $PDMPOH^+$ imaging with data collected over the wavelength range 460-470 nm and (c) bright field image of same sample. The numbers indicate exposure to PDMPO: the sample without PDMPO (1), the sample after 2 hours of PDMPO exposure to PDMPO (2), the sample after 4 hours of PDMPO exposure (3), the sample after 22 hours of PDMPO exposure (4) and the fluorescence emission spectra over time (5). Images in Figure 1(a) and column (b) have had their brightness enhanced to visualise objects present and are not representative of the actual levels of fluorescence over the selected wavelength range.

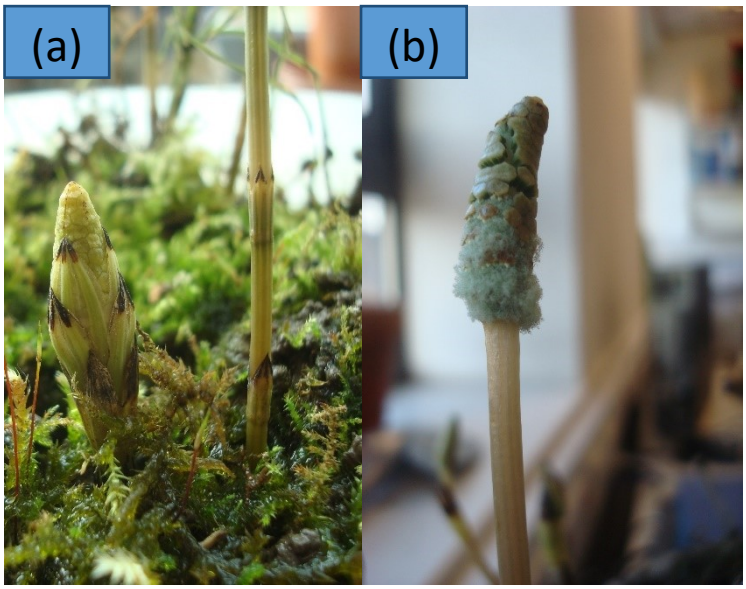

Figure S8: Images of developing *Equisetum arvense* plants including (a) the fertile spore head and (b) fully formed spores ready for ejection (b). The spore head is ca. 1cm in diameter.

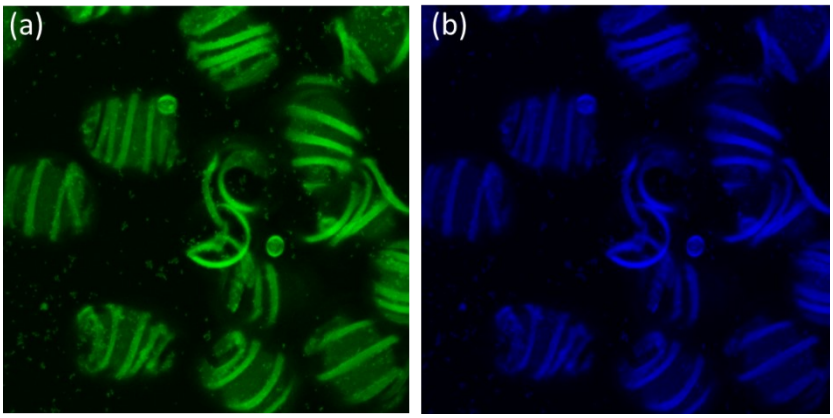

Figure S9: *Equisetum arvense* spores. (a) $(PDMPOH_2)^{2+}$ imaging with data collected over the wavelength range 500-510 nm, (b) $PDMPOH^+$ imaging with data collected over the wavelength range 460-470 nm. The colours in (a) and (b) are false colours put through ImageJ to the greyscale images before the dividing step in the processing. The level of dye uptake over an extended period was sufficient to easily visualise the objects present.

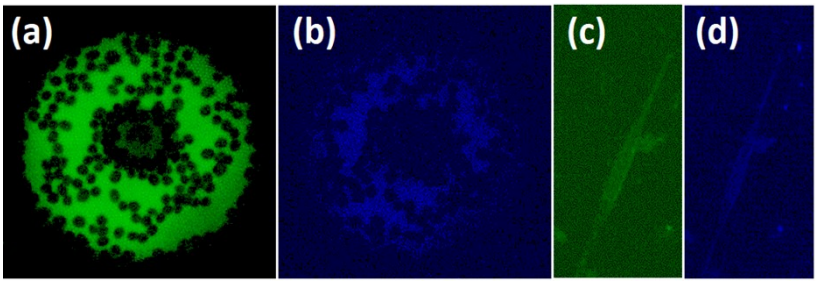

Figure S10: For diatoms *Coscinodiscus Wailesii* and an exemplar freshwater diatom: (a) and (c) $(PDMPOH_2)^{2+}$ imaging with data collected over the wavelength range 500-510 nm, (b) and (d) $PDMPOH^{+}$ imaging with data collected over the wavelength range 460-470 nm. The brightness of all images has been increased to enhance visibility. The level of dye uptake was very low but this did not prevent a ratiometric analysis of the silica structures present as per Figure 6 in the main text.

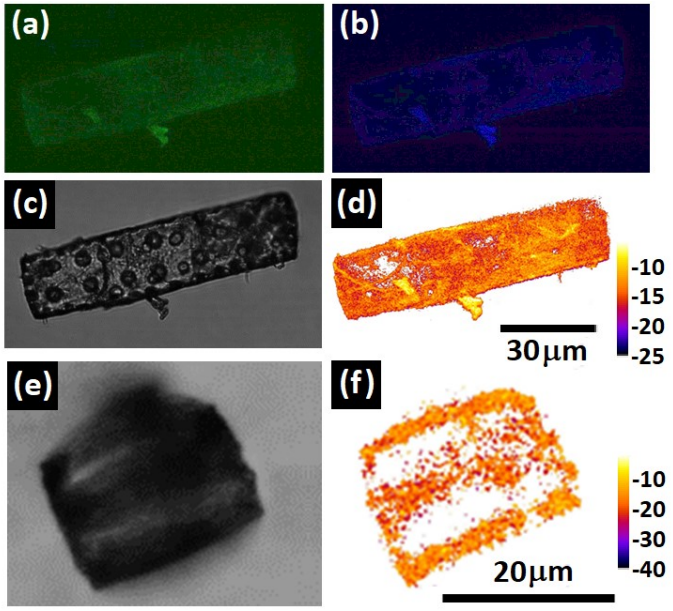

Figure S11: Functional imaging on two freshwater diatoms. Top 4 images *diatoma mesodon* and bottom two images diatom *vulgaris bory* (a) $(PDMPOH_2)^{2+}$ imaging with data collected over the wavelength range 500-510 nm, (b) $PDMPOH^{+}$ imaging with data collected over the wavelength range 460-470 nm, (c) bright field image of the same sample and, (d) effective zeta potential image calculated from the ratiometric processing of $(PDMPOH_2)^{2+}$/ $(PDMPOH)^{+}$ using ImageJ. (e) bright field imaging of diatom *vulgaris bory* and (f) corresponding ratiometric image. The colours in (a) and (b) are false colours put through ImageJ to the greyscale images before the dividing step in the processing. Images (a) and (b) have had their brightness increased to aid visualization of the diatom. Note, the low uptake of dye did not prevent ratiometric analysis of the silica structures present.

Additional References:

i. Goldstein, D. Effect of alcohol on cellular membranes. *Annals of Emergency Medicine*, **1986**, 15(9), 1013-1018.

ii. Maxwell, K.; Johnson, G. Chlorophyll fluorescence—a practical guide. *Journal of Experimental Botany*, **2000**, 51(345), 659-668.

iii. Patra, M.; Salonen, E.; Terama, E.; Vattulainen, I.; Faller, R.; Lee, B.; Holopainen, J.; Karttunen, M., Under the Influence of Alcohol: The Effect of Ethanol and Methanol on Lipid Bilayers. *Biophysical Journal*, **2006**, 90(4), 1121-1135.

iv. Pedrós, R. ; Moya, I.; Goulas, Y. ; Jacquemoud, S., Chlorophyll fluorescence emission spectrum inside a leaf. *Photochemical & Photobiological Sciences*, **2008**, 7(4), 498-502.